JOURNAL OF MORPHOLOGY 268:50–63 (2007)

Morphological Changes in Pedal Phalanges Through Ornithopod Dinosaur Evolution: A Biomechanical Approach

Karen Moreno,[1]* Matthew T. Carrano,[2] and Rebecca Snyder[3]

[1]*Department of Earth Sciences, University of Bristol, Bristol BS8 1RJ, UK*
[2]*Department of Paleobiology, National Museum of Natural History, Smithsonian Institution, Washington, District of Columbia 20013-0121*
[3]*Applied Morphometrics Laboratory, National Museum of Natural History, Smithsonian Institution, Washington, District of Columbia 20013-0121*

ABSTRACT The evolution of ornithopod dinosaurs provides a well-documented example of the transition from digitigrady to subunguligrady. During this transition, the ornithopod pes was drastically altered from the plesiomorphic dinosaurian morphology (four digits, claw-shaped unguals, strongly concavo-convex joints, phalanges longer than wide, excavated collateral ligament fossae, presence of sagittal ridge, and prominent processes for the attachment of tendons) to a more derived condition (tridactyly, modification of the unguals into hooves, phalanges wider and thinner than long, lack of collateral ligament fossae, loss of sagittal ridge and tendon attachment processes, relatively flattened articular surfaces). These changes are particularly noteworthy given the overall conservatism in pedal morphology seen across Dinosauria. But what are the functional consequences of these specific morphological transitions? To study them, we examine a wide range of pedal morphologies in four non-avian dinosaurs and two birds. Our analyses of the external morphology, two-dimensional models (using Finite Element Analysis), and internal bone structure demonstrate that this evolutionary shift was accompanied by a loss of digit mobility and flexibility. In addition, pedal posture was modified to better align the pes with the main direction of the ground reaction force, thus becoming well suited to support high loads. These conclusions can be applied to other, parallel evolutionary changes (in both dinosaurs and mammals) that involved similar transitions to a subunguligrade posture. J. Morphol. 268:50–63, 2007.

KEY WORDS: biomechanics; functional morphology; kinematics; foot; finite element analysis; trabecular structure; stress distribution

Ornithopods were a diverse group of ornithischian dinosaurs that, having originated as approximately kilogram-sized bipeds in the Late Triassic, eventually achieved multi-ton body sizes by the Late Cretaceous. The development of cranial crests among hadrosaurid ornithopods is one of the most remarkable aspects of their evolutionary history (Sereno, 1999). The group is particularly interesting from an evolutionary standpoint because it records a number of long, gradual morphological transitions via a relatively dense series of closely related forms. Among the most significant such transitions is the acquisition of quadrupedalism, associated with many modifications of the pes (Fig. 1).

The acquisition of a subunguligrade pes presents a striking example of convergence with mammals such as rhinocerotids and proboscideans. Studies of mammals indicate that as body size increases, limb posture becomes progressively more upright, and limb motion is restricted to a predominantly parasagittal plane (Hildebrand, 1988; Biewener, 1989; Christiansen, 2002). These changes allow a reduction in the mass-specific amount of force required to counteract moments about the limb joints (Biewener, 1989), and are based on physical rather than phylogenetic constraints. Therefore, it is reasonable to hypothesize that such changes may have accompanied body-size increases in dinosaurs as well.

In fact, the transition to a quadrupedal posture occurs in parallel within numerous dinosaur lineages [stegosaurs, ceratopsians, and sauropods (Sereno, 1999; Carrano, 2001)], presumably with a consequent forward shift of the center of mass (Henderson, 1999). Although some uncertainty still exists about how specialized (or obligatory) ornithopod quadrupedalism was, evidence of its use is available from different-sized manual/pedal sets of footprints (Lockley and Hunt, 1995; Wright, 1999). In addition, the more primitive ornithopod *Dryosaurus* may represent an intermediate stage in the transition to bipedalism, in which juveniles engaged in facultative quadrupedalism but

Contract grant sponsors: NMNH Equipment Fund; Overseas Research Student Award, Universities UK; University of Bristol Scholarship; Evolution of Terrestrial Ecosystems Group (publication no. 141).

*Correspondence to: Karen Moreno, University of New South Wales, School of Biology, Earth and Environmental Sciences, Biology Building (D26), Room 558, Sydney, Australia 2052.
E-mail: dinohuella@yahoo.com

Published online 4 December 2006 in
Wiley InterScience (www.interscience.wiley.com)
DOI: 10.1002/jmor.10498

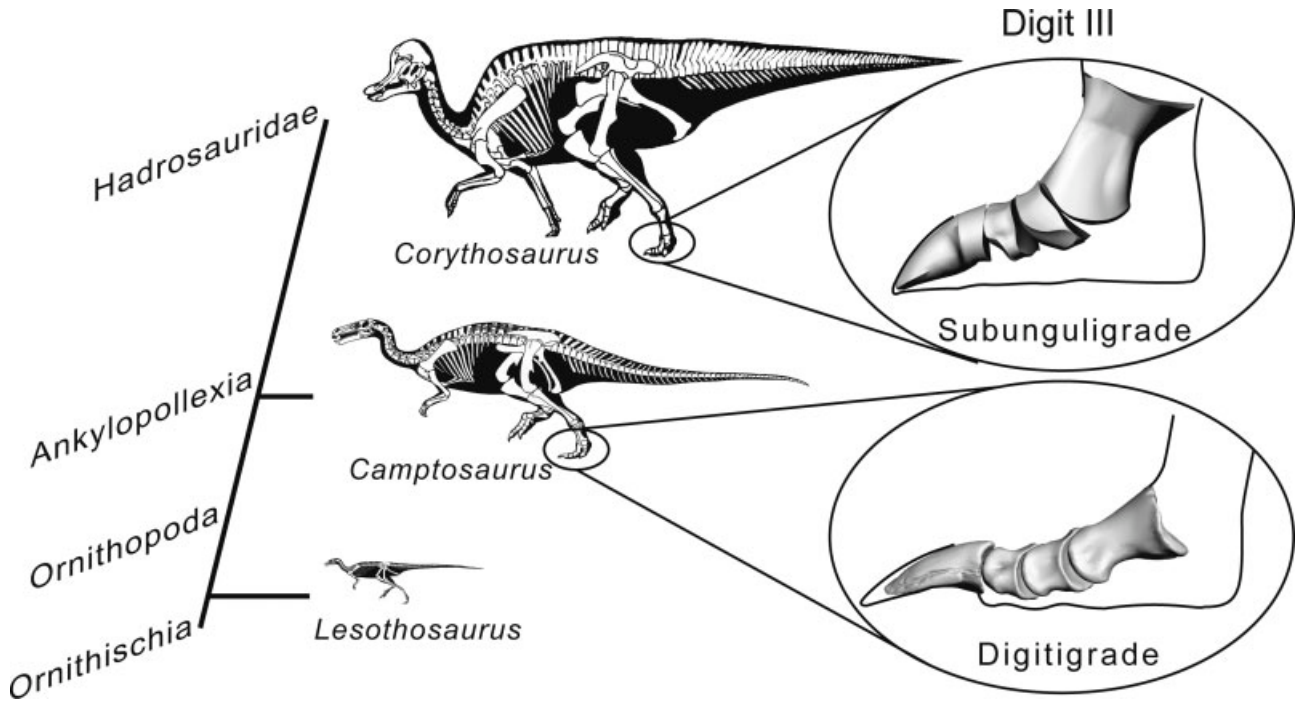

Fig. 1. Evolution within Ornithopoda. Changes of stance, posture, and size are evident from the skeletal reconstructions; enlargements highlight changes in digit III pedal morphology. The presence of a soft-tissue pad (black outline beneath pedal phalanges) has been inferred from trackway morphologies. Skeletal reconstructions are approximately to scale (*Lesothosaurus*, 1 m total length; *Camptosaurus*, 8 m; *Corythosaurus*, 10 m; modified from Paul 1987); (phylogeny simplified from Carrano, 1999).

adults were nearly exclusively bipedal (Heinrich et al., 1993). A comparative anatomical study of the hadrosaurid ornithopod *Maiasaura* (Dilkes, 2001) showed that although the forelimb was gracile, it was well suited to carry a portion of body weight, especially in adults.

The pedal morphology of basal ornithopods is shared with theropods and is considered plesiomorphic for Dinosauria. This morphology consists of three primary weight-bearing digits, a phalangeal formula of 2-3-4-5-0, claw-shaped unguals, phalanges that are proximodistally longer than mediolaterally wider, well-developed collateral ligament fossae (Fig. 2A), prominent proximal processes for the attachment of extensor and flexor tendons, and pronounced development of saddle-shaped (or ginglymoid) joints formed by a sagittal ridge on the proximal phalangeal articular surface (and a complementary furrow on the distal surface) (Fig. 2B). These features are evident in most basal ornithischians, including *Lesothosaurus* and "hypsilophodontians" such as *Hypsilophodon*, *Thescelosaurus*, and *Tenontosaurus*. Basal ankylopollexians such as *Camptosaurus* show some forelimb modifications that suggest intermittent use in support, but the pes remains quite primitive and retains three claw-like unguals.

In all these forms, the pes is distinctly digitigrade, and footprints attributed to primitive ornithopods show discrete digit marks with no indication of a fleshy metatarsal pad. However, more highly derived ornithopods (iguanodontians) modified this digitigrade pes into a more subunguligade structure. At the same time, the manus became more highly modified for weight bearing, and quadrupedalism was presumably more frequently used. These ornithopods eliminated the first pedal digit (resulting in a phalangeal formula of 0-3-4-5-0) and modified the unguals into hooves. The phalanges are mediolaterally wider and anteroposteriorly thinner than proximodistally long, lack collateral ligament fossae, and exhibit neither a sagittal ridge, a process for tendon attachment, nor excavation of the joint surfaces; all articular surfaces are flattened relative to the plesiomorphic state. These marked postural and morphological differences imply associated differences in pedal kinematics, and therefore in the distribution of forces across the pes.

In the present work, our goal was to evaluate the responses of different ornithopod phalangeal morphologies to external loading. Specifically, we examined differences in pedal digit morphology and mobility within and among taxa by studying the external characteristics of the joints. To test whether these differences may have been correlated with loading conditions during locomotion, we modeled the distribution of loading in isolated phalanges of various proportions using finite element analysis (FEA). Because trabecular architecture is at least partly related to the principal lon-

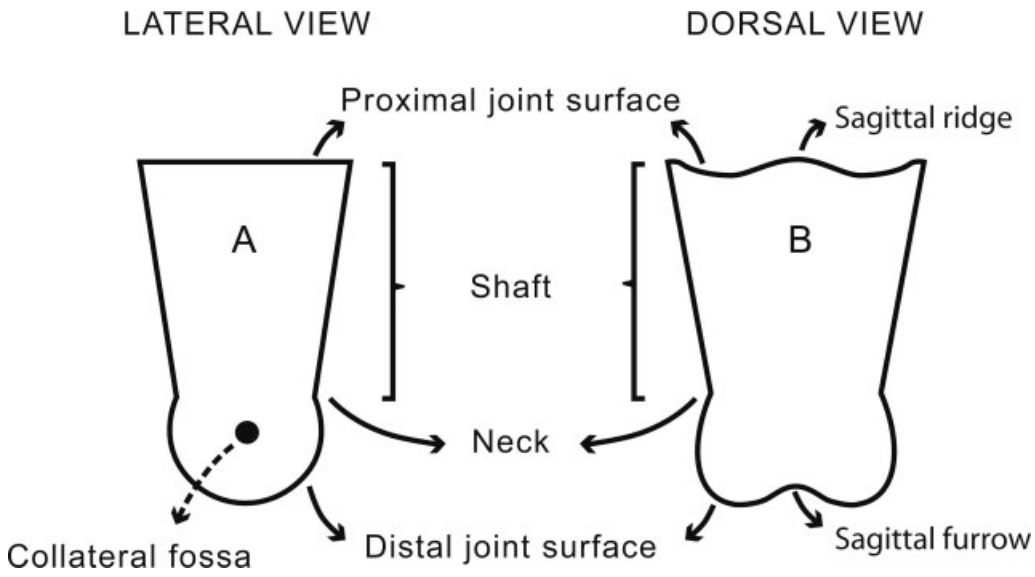

Fig. 2. Anatomical terms and measurements used in this study. **A**) Mediolateral view; **B**) Anterior view.

gitudinal stresses and the magnitude of shear stresses (Wolff, 1870; Hayes et al., 1982; Bertram and Swartz, 1991; Gefen and Seliktar, 2004), we documented the internal trabecular structure using computed tomography (CT) scanned images, and made comparisons to the modeled loading patterns. Finally, we interpreted the results in light of several perceived anatomical "zones" within the phalanx, as a means to understand the consequences of morphological changes on the external and internal structures of the distal pedal phalanges.

MATERIALS AND METHODS

For this study, we focused on the non-ungual phalanges from nearly complete specimens of associated ornithopod feet. We studied three specimens of the ankylopollexian *Camptosaurus dispar* (USNM 5473, USNM 4277, USNM 4697) and two hadrosaurids, *Corythosaurus casuarius* (USNM 15578) and *Saurolophus sp.* (AMNH 5271; mounted in plaster). For comparative purposes, we also examined the pedes of the non-avian theropod *Allosaurus fragilis* (USNM 8324) and the extant ratites *Dromaius novaehollandiae* and *Rhea americana* (Fig. 3).

External Morphology

We quantified the distal joint curvature (Fig. 4A) and sagittal ridge height (Fig. 5A) of the pedal phalanges in order to describe the basic changes that occurred during the evolution of the ornithopod pes. Joint curvature reflects the maximal amount of dorsoventral flexion and extension; more flattened phalangeal surfaces were presumably capable of less rotation in the dorsoventral plane. The sagittal ridge is a narrow crest that crosses the proximal joint surface dorsoventrally, dividing it into two concave facets and thereby creating a ginglymoid morphology (Fig. 2B). This morphology at least partly serves to constrain mediolateral and rotational movements, acting to enforce dorsoventral motion when the joint is under torsional loads.

Measurements of the sagittal ridge and joint curvature on these specimens were obtained from the digitized distal joint surfaces using a MicroScribe G2XL (Immersion Corporation M.R.) in combination with the software Rhinoceros 3D (version 3.0, educational license for the Applied Morphometrics Laboratory, National Museum of Natural History, Smithsonian Institution). For practical reasons, the sagittal ridge data were collected from the distal joint surface (i.e., the sagittal furrow) of the preceding phalanx (Fig. 2B). Although the sagittal ridge itself is present on the proximal articulation, the contacting phalangeal surfaces conform nearly perfectly, permitting accurate measurements to be taken from either surface.

Modeling

We created two-dimensional (2D) models of individual phalanges with the software Fempro (Algor V19, Fempro). We constructed basic phalangeal models by assembling two basic geometric shapes, a circle and a truncated cone, into a single structure that represents a phalanx in lateral view. Either shape (or both) could be modified in order to create variations in the overall shape of the phalanx.

Constant left-right symmetry of the structure (circle and truncated cone assembled) was maintained in our models (Fig. 2A). Although real phalanges often show some degree of asymmetry, especially in animals with specialized locomotory behaviors (e.g., asymmetrical step, fossorial, etc.), the objective of our model is to show general patterns in phalangeal morphology that can be easily compared between different animals regardless of individual or specific variations. The different degrees of asymmetry can be treated as an additional (untested) variable that might further modify the stress distributions; certainly this aspect is worthy of further study.

The scale of the model is assumed to have little effect on the stress distribution. Other studies have shown that for many mammals, stresses are maintained at relatively constant levels over a wide size range without disproportionate changes in the cross-sectional areas of bones (Alexander et al., 1979). Therefore, the results of the present model can be generally compared with pedal bones of different absolute sizes.

To study the influence of shaft length (Fig. 2A), we increased the height of the truncated cone, but not the dimensions of its top, bottom, sides, or of the circle. We used the same method to vary the proximal surface width, by changing the length of the topside of the truncated cone and adjusting the lateral sides for

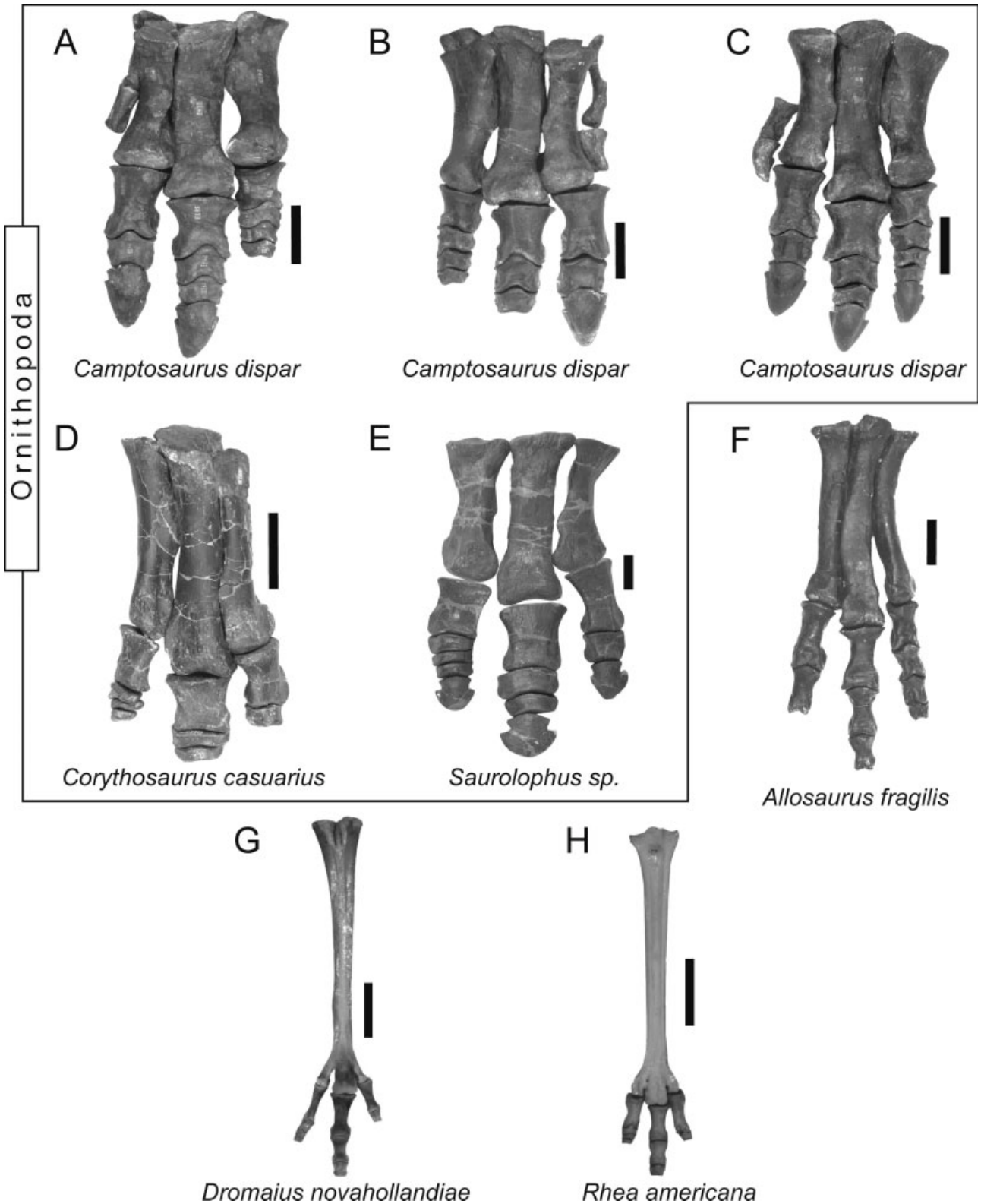

Fig. 3. Photographs of specimens used in this study in dorsal view. **A**) *Camptosaurus dispar*, left pes, USNM 5473; **B**) *Camptosaurus dispar*, right pes, USNM 4277; **C**) *Camptosaurus dispar*, left pes, USNM 4697; **D**) *Corythosaurus casuarius*, right pes, USNM 15578; **E**) *Saurolophus sp.*, right pes, AMNH 5271; **F**) *Allosaurus fragilis*, left pes, USNM 8424; **G**) *Dromaius novaehollandiae*, left pes, P. Kroehler, pers. coll.; and **H**) *Rhea americana*, right pes, P. Kroehler, pers. coll. Ornithopods are enclosed in a frame. Scale bars = 10 cm.

the new shape. For the proximal joint concavity, the portion enclosed by a curve inscribed within the truncated cone was subtracted from the total surface. An equivalent technique was used for the distal convexity: we subtracted the distalmost area formed by a curve inscribed in the circle.

Finite Element Analysis

We performed a FEA in order to examine stress distributions within the modeled phalanges. The FEA was performed by the software Fempro (Algor V19, Fempro), under the following conditions:

1) Meshing was set to triangular shape at a density of 400–450 triangles per area unit, with optimum meshing symmetry. This construction geometry acts as a braced framework (truss), preventing bending loads in the structure, and is subjected only to longitudinal loading (tension and compression) but not shear or bending. These characteristics are compatible with cancellous bone behavior (Currey, 2002; Levin, 2002).
2) Material properties were taken from published values (Reilly and Burstein, 1975) for fast-growing Haversian bovine bone (isotropic): density = 1,895 kg/m^3; elastic modulus (E) = 10 GPa; Poisson's ratio = 0.4; shear modulus (G) = 3.66 GPa. Bovine histology seems to resemble that of certain dinosaurs (Reid, 1996), at least enough to allow the assumption of broadly similar material properties and minimum strength capability estimates for the models.

   Nonetheless, we also tested two other material properties in order to assess the effects of changes in this variable. First, we used general bone material properties taken from Currey, 2002: density = 2,000 elastic modulus (E) = 20 GPa; Poisson's ratio = 0.3; shear modulus (G) = 5 GPa. Using these properties did not affect the stress distribution; minimum and maximum stress values varied up to 3% from the calculated ones using bovine material, but retained their linearity. Second, we used red oak wood (the optimum under compression) from Algor's Library (density = 662.6 elastic modulus (E) = 12.411 GPa; Poisson's ratio = 0; shear modulus (G) = 0 GPa). This test also confirmed stress distribution and linearity, with output values (stress) deviating up to 8% in comparison with Bovine material. Both of the alternative materials tested do not alter the general results of our study. Therefore, there is no reason to believe that biologically reasonable changes in material properties would modify our conclusions.
3) With estimates of the body weight and the proximal joint surface area of a given bipedal tridactyl dinosaur, one can roughly calculate the loading conditions on a single toe in a standing still posture. *Camptosaurus* and *Allosaurus* had a body weight of ~10 kN (calculated based on femoral circumferences ~300 mm for USNM 6061, USNM 5959, and USNM 8424; Anderson et al., 1985) and a proximal joint surface area of ~30 to 40 cm^2. *Corythosaurus* and *Saurolophus* had a body weight between 70 and 100 kN (Seebacher, 2001), and a proximal joint surface of 50–60 cm^2. Using these estimates, we derive for a single toe a load of ~0.5 MPa (1 MPa = 1,000 kN/m^2) for *Camptosaurus* and *Allosaurus*, and a load of 2–3 MPa for *Corythosaurus* and *Saurolophus*. These values fall well within the range of values tested in our models (between 0.0001 and 300 MPa). It is important to mention that the resultant stress is actually a linear function of the applied load. In other word, the stress distribution is independent of the load magnitude itself. Therefore, even if the estimates above for realistic loading conditions (0.5–3 MPa) are inaccurate, our results remain valid.

   Loading was applied normal to the joint surface, under the assumption that the cartilage and synovial capsule would transmit most normalized forces. This is based on theoretical models (Matthewson, 1982; Dar and Aspden, 2003), which establish that the synovial liquid (uncompressible) as well as the cartilage elasticity redistributes and homogenizes loads. Real conditions might differ from theoretical ones, and are worth further study, but these conditions are used here to facilitate calculations in the present study.
4) Mobility was constrained by fixing the distal joint in all directions (Fig. 2A), in order to simulate limitations on movement due to the presence of a subsequent phalanx, the ground reaction force (GRF), and the collateral ligaments when the foot was in contact with the ground. Tendon force was not considered in the study, because it would introduce a dynamic structure, thus beyond the scope of the present analysis.
5) Output stress values are expressed as a percentage of the load applied. This method permits a correct interpretation of the data, since the numbers presented here have little relationship with other experimental or in vivo values. Stress values (Von mises) can be obtained simply by multiplying the magnitude of the load in N/m^2 applied and dividing by 100. Values were tested between 1,000 and 300,000,000 N/m^2 (see above).
6) For all FEA results, color range settings were standardized based on the highest and lowest percentages found after all the model calculations were completed (27–338%). This provides a visual means for comparing communicating stress distributions between the models.

These loading and constraint conditions correspond to a static analysis of the stance phase in locomotion. As the phalanges were modeled as isolated elements, and loading magnitude and direction have no significant effect, our model will reveal general stress distributions for any phalanx at a given instant when the foot is in contact with the ground. This means that our modeled phalanges could correspond to any location in the foot (different phalanges, digits, or sides), as well as different foot postures during weight-bearing walking phases (early stance, weight bearing, kick off), but always (and only) under static conditions.

Internal Morphology

We obtained images of the internal structure of the bones by CT scanning, using a Somatom AR.SP scanner (Siemens Corporation) at the National Museum of Natural History (Smithsonian Institution). We scanned the first pedal phalanges of four taxa: *Allosaurus*, *Camptosaurus*, a juvenile *Corythosaurus*, and *Saurolophus*. The first three were scanned using a consistent field of view (FOV) of 116 mm^2 (512 × 512 voxels) and 1 mm slice thickness. The single specimen of *Saurolophus* (AMNH 5271) required a larger FOV of 350 mm^2 (512 × 512 voxels) and 2 mm slice thickness because it was permanently mounted on a plaster base.

These images revealed the general trabecular orientation and density of the internal structure of the bones, which are known to have some relationship with the orientation of principal compressive or tensile stresses, as well as the magnitude of shear stresses (Wolff, 1870; Hayes et al., 1982; Bertram and Swartz, 1991; Gefen and Seliktar, 2004). We tested these observations against independent results from the FEA of two-dimensional models (see above).

In the CT images, the gray scale indicates material density, with white as the highest value and black as the lowest (e.g., Fig. 8). However, it is important to note that high density (white) does not necessarily indicate dense fossilized bone, but could also correspond to a harder element such as quartz (perhaps infilling the medullary cavity), or to a transition between a surrounding low-density material (air) to the higher-density fossil (often creating a white outline).

No extant taxa were included in the current analysis. This deliberate omission reflects the significant anatomical differences between most modern animals and non-avian dinosaurs, which present a specific loading problem in each case and are beyond the scope of the present investigation. For example, birds display a distinct limb orientation in steady standing: a horizontal femur and a near-vertical lower limb, which would

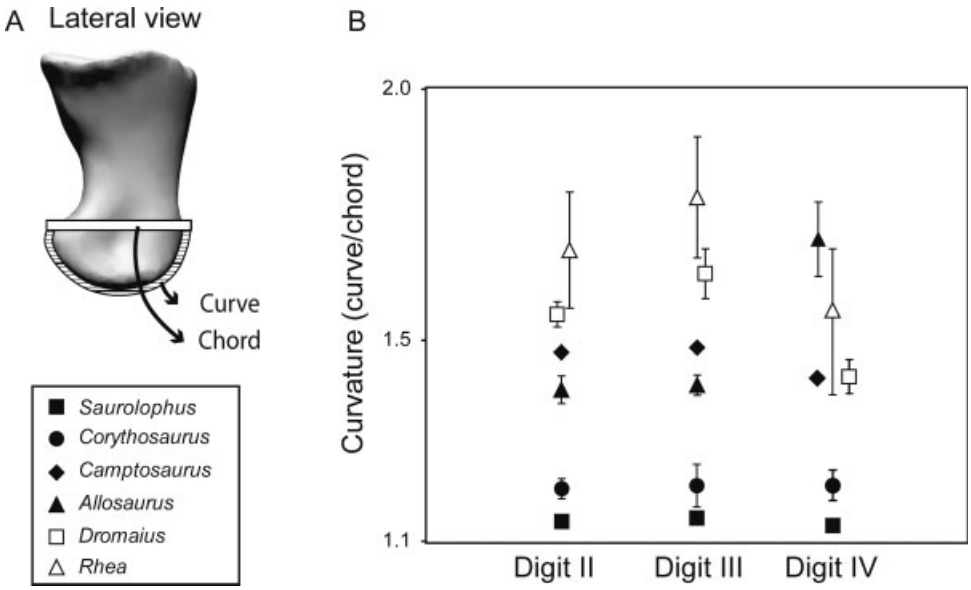

Fig. 4. Distal joint curvature in pedal phalanges. **A**) Measurements taken in lateral view (curve, chord), showing the curvature calculation. **B**) Graph of the average curvature for each digit in the studied specimens.

transmit a large amount of the load from the metatarsal ends to the ground and a minor part to the pes (Carrano and Biewener, 1999; Farlow et al., 2000), thus minimizing the participation of the phalanges in supporting body weight. A different but analogous result would be expected for reptiles due to their sprawling leg posture. Finally, mammals, which seem to have closer limb postures and locomotion biomechanics with dinosaurs (Carrano, 1997, 1998, 2001), exhibit a distinct ankle anatomy, with a greater participation of tarsals rather than phalanges. All these variables require further study and the development of more complex models.

RESULTS

External Morphology

The distal joint curvature is approximately circular in lateral view, and the collateral ligament fossa is located close to the center of rotation (Fig. 4A). However, the penultimate phalanges are an exception; they achieve a larger ventral joint surface through a reduction of dorsal width and increase in ventral width. Here, when the collateral fossa is

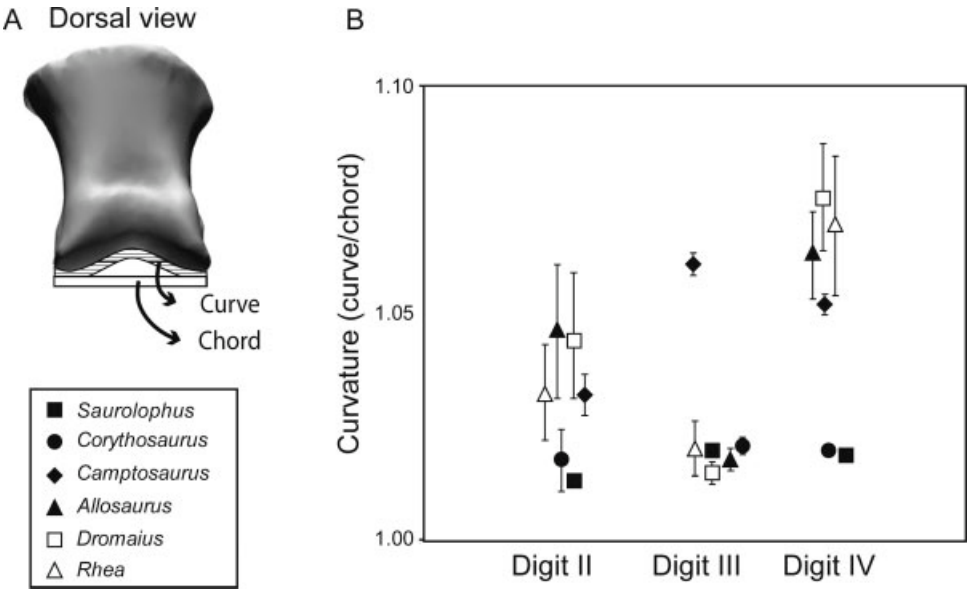

Fig. 5. Joint surface topography in pedal phalanges. **A**) Measurements taken in dorsal view (curve, chord), distal joint surface (sagittal furrow), showing the curvature calculation. **B**) Graph of the average sagittal furrow depth.

present (*Camptosaurus*, *Allosaurus*, and ratites) and displaced dorsally, it generates an angle with respect to the ligament that attaches to the ungual.

The depth of the collateral ligament fossa can be greater on either the lateral (*Camptosaurus*) or medial side (*Allosaurus*), or both may be equal (ratites). On the other hand, *Saurolophus* and *Corythosaurus* lack such fossae, and the distal joint remains roughly symmetrical, although the outer sides are better developed in digits II and IV.

The average curvature (Fig. 4B) of *Corythosaurus* phalanges is nearly constant and close to 1.0 for all three digits. In contrast, digits II and III of *Camptosaurus* seems to be at least as curved as those of *Allosaurus* if not more, but in general curvature remains constant between and within digits (a low standard deviation). *Allosaurus* has one of the largest digit IV curvatures, even more than the average in birds, whereas birds have the largest distal joint curvatures in digits II and III. Ratites show a large standard deviation in all digits. This reflects the high curvature of proximal phalanges and relatively lower curvature of distal phalanges. In Figure 4B, *Dromaius* and *Rhea* plot together within the same standard deviation.

For most taxa we examined, lateral digits have a wider dispersal of values than the central one (Fig. 5B), and show a better-developed sagittal ridge. This is especially the case for digit IV, where we found the greatest depth values. With the exception of *Camptosaurus*, the third digit presents a low sagittal ridge, and all digit III phalanges plot together. *Corythosaurus* and *Saurolophus* retain low depth values for all digits, which is indicative of their derived hadrosaurid condition (i.e., flattened joint surfaces).

To summarize, the phalangeal curvature (characteristic associated with movement range) and the development of the sagittal ridge (related to phalangeal interlocking) show a general decrease in the following order: first theropods (*Allosaurus* and the birds) together with *Camptosaurus,* and finally hadrosaurids. An exception to the rule is digit III of *Camptosaurus*, which has a deep sagittal ridge and contrasts with all the other taxa examined. Curvature is consistent between the digits in ornithopods, whereas it shows greater variability in theropods.

Finite Element Analysis 2D

In general, our 2D FEA models exhibit their highest stress zones at the contact between the truncated cone and circle (i.e., the phalanx neck; Fig. 6), where the extremes of the constraints are located. The lowest stresses are distributed toward the distal joint. Logically, these stress patterns are highly influenced by the geometric properties of the phalanx. The cone acts as a funnel, concentrating loads toward the outside edges of the narrow section, and the circle efficiently focuses them near the loading point, which is evident in the model results (see Fig. 6). Even when these geometric figures are fused, with smooth edges, the stress distribution pattern remains fairly constant (Fig. 7.1B,D).

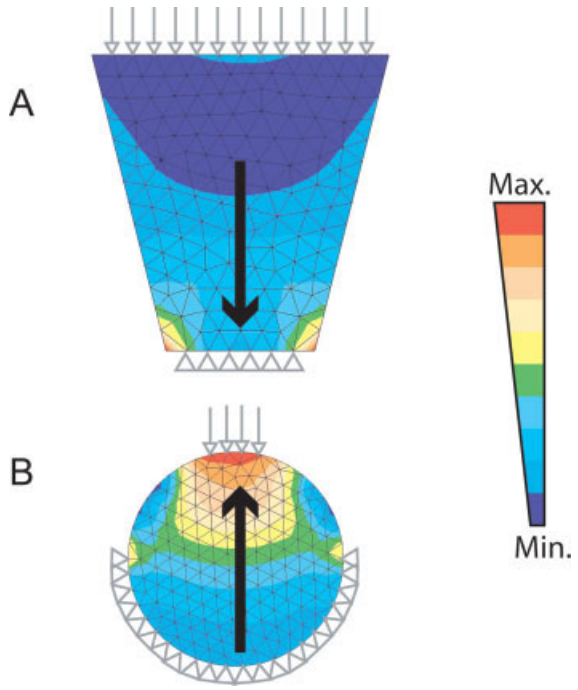

Fig. 6. Stress distribution in the basic geometrical shapes used to construct our 2D phalanx model. **A**) Truncated cone; **B**) Circle. Gray arrows show the application of stress; gray triangles indicate where the structure was fixed against motion. Internal stress levels are shown from highest (red) to lowest (blue). Note that the truncated cone concentrates stress toward the distal part, whereas the circle effectively concentrates it near the point of application (black arrows).

Shortening the shaft length (Fig. 7.1A–D) increases the maximum stress (compare between Figs. 7.1A,C and 7.1B,D) but tends to lower the minimum stress. Therefore, the range of stress values is wider, and high loads are concentrated in the small area of the phalanx neck (see Fig. 2); this region exhibits the highest stress of all the experimental models (Fig. 7.1C).

Small increases in the concavity of the proximal joint surface (Fig. 7.2A–D) generate a small decrease in maximum stress (Fig. 7.2B,C), but a deeper concavity with sharp edges produces higher stress along this surface (Fig. 7.2D). Hence, the potential benefits (lower stress range) of increasing the proximal concavity are limited. Minimum stress remains constant and distally located, which means that changes to the morphology of the proximal concavity have no effect on the distal joint surface, in contrast to the previous example. These models also show larger stresses distributed along the walls, leaving

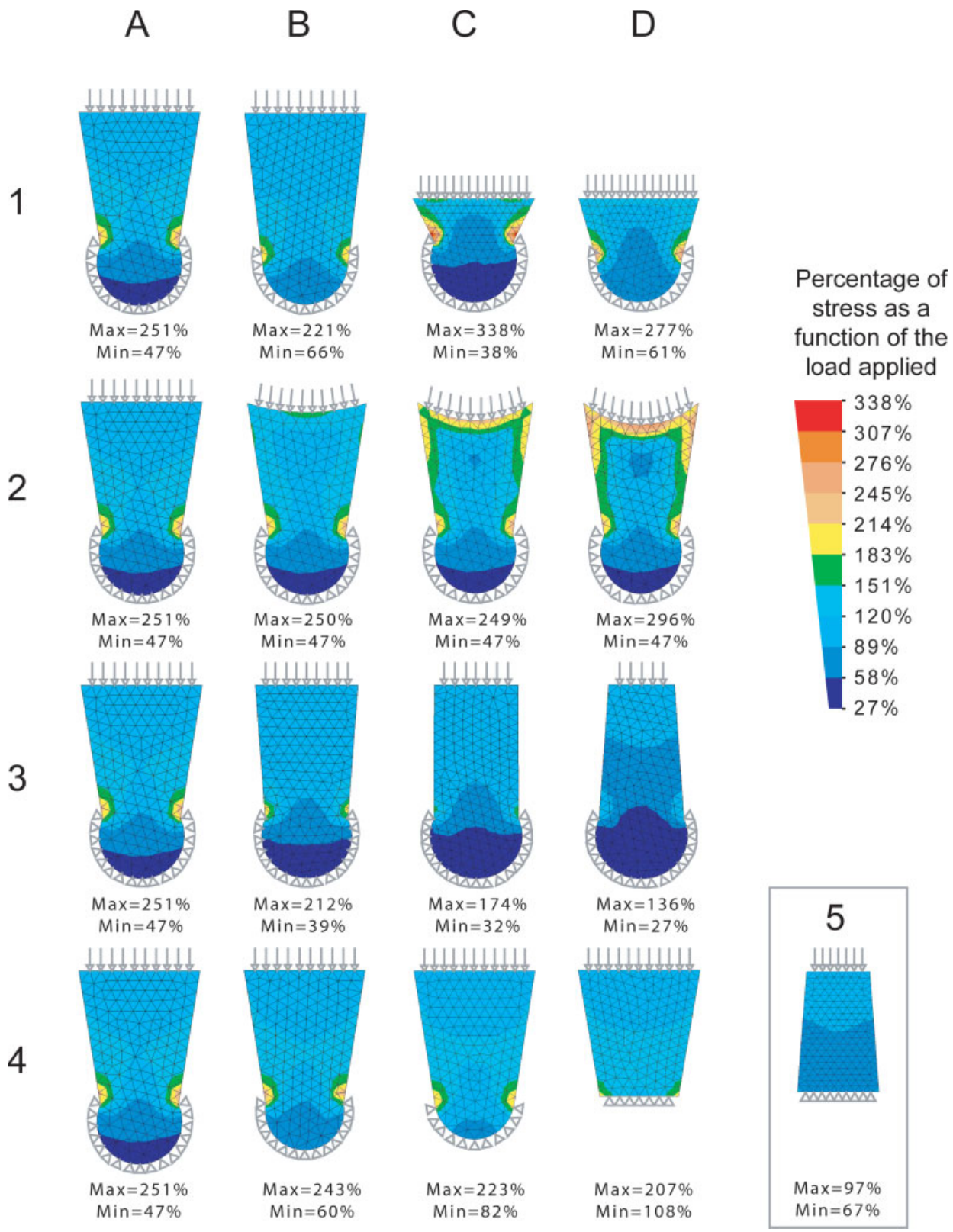

Fig. 7. 2D model of a phalanx in FEA, showing effects of morphological variation. Row **1** varies shaft length and "neck" presence: 1**A**) original shape, considered a "long shaft"; 1**B**) removal of "neck" from original shape; 1**C**) shortened shaft; 1**D**) shortened shaft without "neck". Row **2** (**A–D**) varies the depth/curvature of the proximal concavity. Row **3** (**A–D**) demonstrates a decrease in the proximal joint width. Row **4** (**A–D**) demonstrates a decrease in the distal joint convexity. Row **5** shows the effect of combining narrow proximal width (3D) with flattened distal and proximal joints (4D). Column A represents the same model in each row, for ease comparison.

an internal region with low stress; this was not observed in any of the other experiments.

The reduction of proximal joint surface width causes a general decrease in stress (Fig. 7.3A–D), which becomes more evenly distributed along the shaft. This experiment caused the greatest overall reduction in stress.

Reducing the convexity of the distal joint surface (Fig. 7.4A–D) raises the minimum stress but slightly decreases the maximum stress. Therefore, a flat structure produces higher but more evenly distributed stresses.

When the two last characteristics are combined, decreasing the proximal concavity and the distal convexity (Fig. 7.5), the resulting stress has a very low range. This variation exhibited the lowest maximum stress of all the experiments.

Internal Morphology

From proximal to distal, the sagittal sections of *Allosaurus* (Fig. 8.1A) and *Camptosaurus* (Fig. 8.2A) phalanges show a conical structure with thick walls of compact bone. This structure is filled internally by a gradient of small (proximal) to large (distal) trabeculae, which give way to a large medullary cavity (mc; Fig. 8.1A,B, 8.2A,B). Both distal joints reveal evenly distributed trabeculae. Bone layering can be observed within either dorsoventral section of the midshafts (Fig. 8.1B, 8.2B). The only difference is the shape of the dorsoventral cross-section, which is kidney-shaped in *Camptosaurus* and circular in *Allosaurus*.

It is important to note that *Allosaurus* shows no major internal structures in CT images (Fig. 8.1). Unfortunately, the specimen was longitudinally drilled to insert a metallic support, and hence was highly fractured. These factors resulted in an altered CT image, in which the conical gradient of the proximal trabeculae is only slightly noticeable. However, it was possible to examine its internal bone architecture by direct observation of the broken parts as isolated elements. This direct evidence shows an internal structure that is similar to *Camptosaurus*.

Corythosaurus (Fig. 8.3A) has an internal structure with more evenly distributed trabeculae than *Allosaurus* and *Camptosaurus*. Although the trabeculae also form a smooth conical gradient, the medullary cavity and compact bone are absent. Large trabeculae lie near the edges of the bone (Fig. 8.3B), and no layering can be identified.

Saurolophus (Fig. 8.4A,B) reveals much more evenly distributed trabeculae than the other specimens, with no conical gradient. The sagittal section (Fig. 8.4A) shows a small zone in the internal part of the midshaft that contains slightly larger trabeculae, but a clear medullary cavity is lacking. In the dorsoventral section, one "layer" passes parallel to the shaft edge and disappears near either joint (Fig. 8.4B). This layer may be a scanning artifact: the plaster mounting adds another material interface, which could have produced additional X-ray reflection/refraction. However, observations of broken hadrosaurid phalanges (phalanx III-3, *Edmontosaurus sp.*, UCM 42353) indicate that this dense CT "layer" could correspond to the boundary of a zone with smaller (and therefore denser) trabeculae located along the medial and lateral perimeter. The other narrow dense zone, which runs from the dorsal edge toward the center of the phalanx (Fig. 8.4B), could also be an artifact. Regardless, the salient observation here is that CT images confirm the absence of the medullary cavity and a more homogeneous trabecular size compared with the other dinosaurs.

DISCUSSION

Pedal Mobility and Flexibility

Interpreting the data in terms of the flexion-extension ability of the joints (distal joint curvature; Fig. 4B) and their ability to resist torsional loads (depth of the sagittal ridge; Fig. 5B), we note that *Camptosaurus* retains high digit flexibility, the primitive condition and, hence, more similarity to *Allosaurus* (see Fig. 9). Accordingly, *Camptosaurus* has a well-developed interlocking phalangeal morphology that counteracts torsional loads. This morphology can be observed even in the third digit, whereas the rest of the animals studied (including birds) show a very shallow sagittal ridge. One possible consequence is an asymmetrical step, in which the animal walked with the pes angled or rotated inward (digits III and IV have deeper sagittal ridges than digit II).

In *Allosaurus*, digit flexibility seems generally conservative. Here, digits II and III are less flexible than in the ratites, but digit IV has a remarkable mobility (Fig. 9C, D), exceeding that seen in the birds. The interlocking phalangeal morphology is also well developed in the lateral digits and, in contrast to *Camptosaurus*, suggests a more symmetrical step in *Allosaurus*.

Dromaius and *Rhea* have similar morphologies to one another (see Fig. 2), and therefore their pedal function is approximately equivalent, as is evident from their similar locomotory habits (Abourachid and Renous, 2000). The fourth digit has reduced mobility and shortened phalanges, presumably working as a stiffer element in comparison with the other digits.

On the other hand, *Corythosaurus* (juvenile) and *Saurolophus* have little flexibility in all three digits. This imparts a low resistance to torsion, even in the lateral digits where all the other animals studied have some development of a sagittal ridge. This is typical for a derived ornithopod, and can be explained as a consequence of the more upright position of the pes (Fig. 10). This reorientation

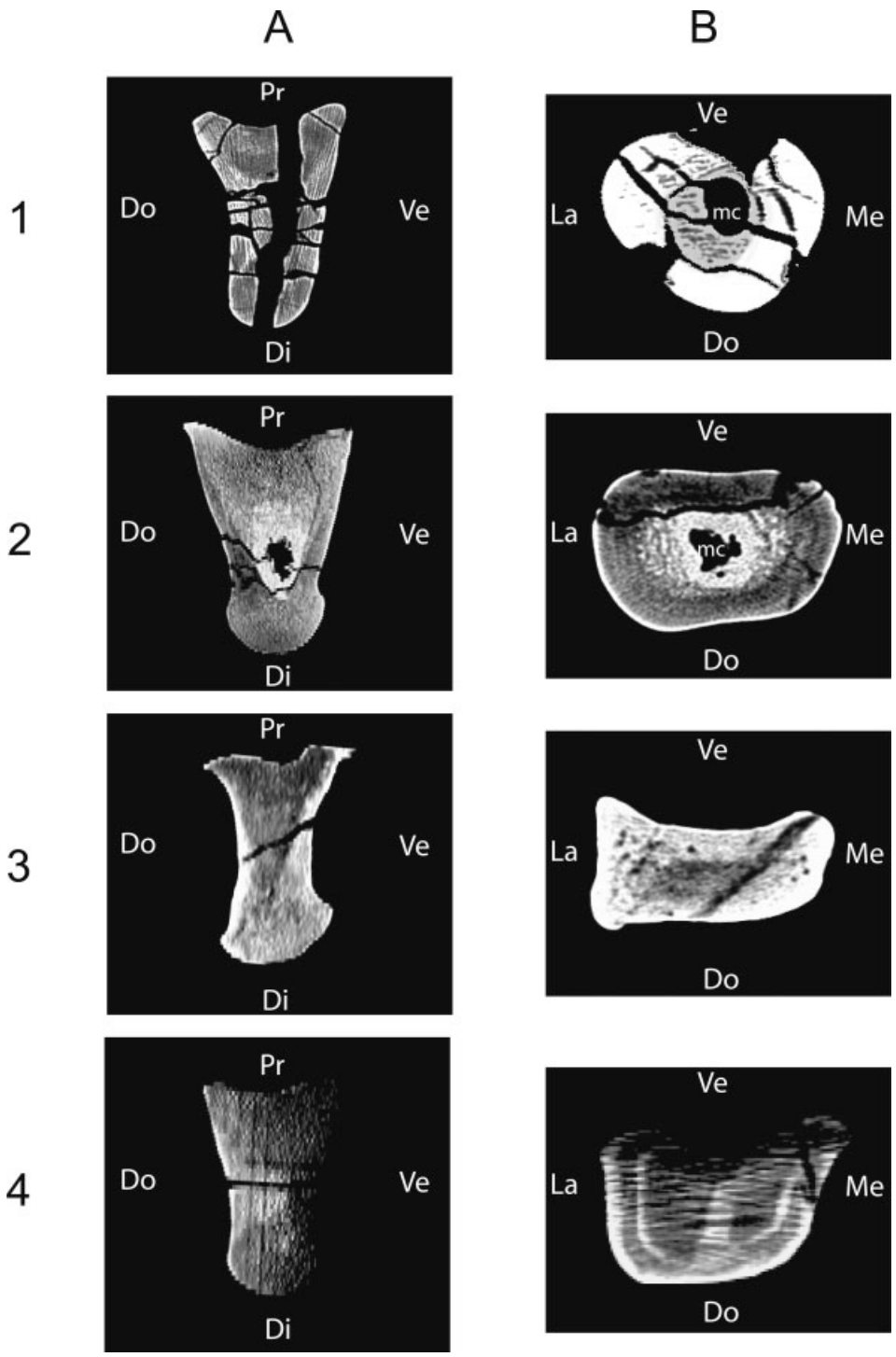

Fig. 8. Internal structure in pedal phalanges in sagittal (**A**) and cross-section (**B**). **1**) *Allosaurus*, second phalanx, digit III; **2**) *Camptosaurus*, first phalanx, digit III; **3**) *Corythosaurus*, first phalanx, digit III; and **4**) *Saurolophus*, first phalanx, digit III. mc = medullary cavity. Not to scale.

aligns the pes closer to the main direction of the GRF, with a resultant loss of digit mobility.

The presence of collateral ligament fossae and their position relative to the distal joint, together with the symmetry of the distal curvature in lateral view, provides additional information about flexion-extension ability. The phalanges studied present symmetrical distal curvature, therefore are built to contribute equally to extension and flexion, and the collateral ligaments constrain and guide their range

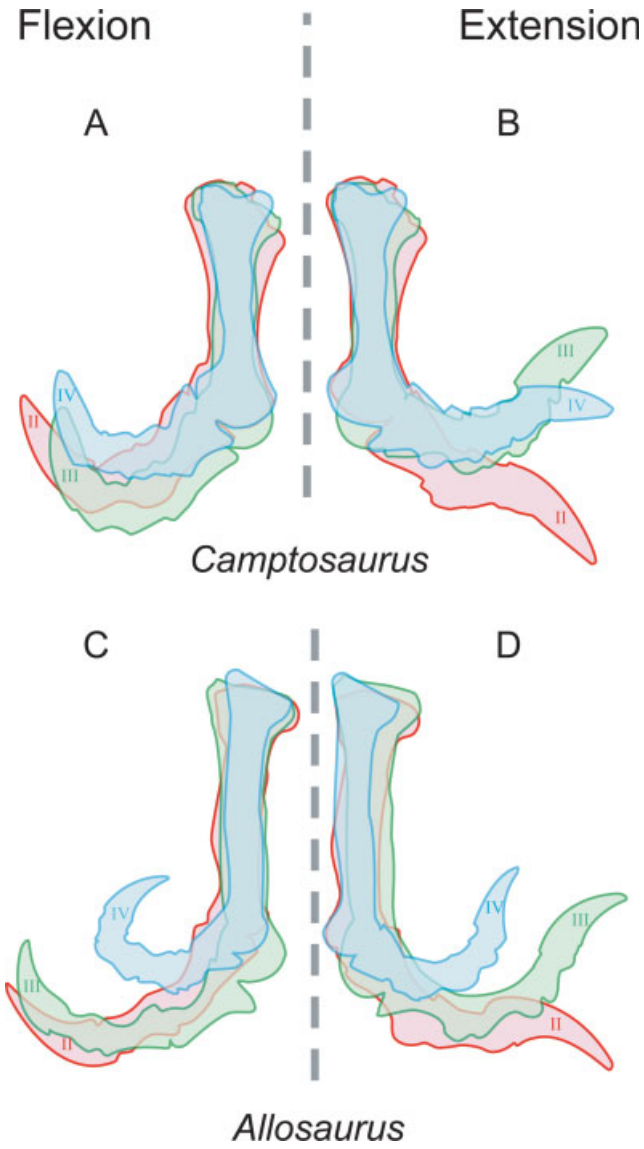

Fig. 9. Reconstructions of pedal mobility using 3D element scans. The pedal phalanges of *Camptosaurus* (**A**, **B**) and *Allosaurus* (**C**, **D**) were placed in maximum flexion (A, C) and maximum extension (B, D). Note that in each case, digit II shows the least mobility, but that the two taxa differ with regard to whether digit III or IV is the most mobile.

of motion. Therefore, movement is restricted dorsally and greater flexion is supported (but extension is reduced) in asymmetrical phalanges, with a better-developed ventral side and more dorsally placed collateral ligament. This is the case for the penultimate phalanges of *Camptosaurus*, *Allosaurus*, and the ratites. Their unguals are probably slightly extended neutrally, with the proximal joint resting high on a footpad, while only a portion of the ungual contacts the ground. The absence of these characteristics in *Corythosaurus* and *Saurolophus* indicates that the ungual is more closely aligned with the preceding phalanx, and therefore less extended neutrally. This suggests a different function of the footpad in hadrosaurids, which evenly supports the entire pes.

Phalangeal Morphology as a Consequence of Pedal Loading

In most of the animals studied, digit III has a very low sagittal ridge (and shallow corresponding furrow) in each of the phalanges (Fig. 5B). The sagittal ridge works to reinforce the dorsoventral rotation of the joint. Its weak development (or absence) indicates that digit III might be subject to low torsional loads, and therefore must be mediolaterally aligned with the GRF. This is confirmed by experiments carried out in starlings and quail (Middleton, 2003), which showed that the center of pressure is in fact located along digit III (which shows a lower sagittal ridge) and the lateral digits act later during the walking phase. Variations of pedal anatomy induced minor changes in the position of the center of pressure, but it always maintained its place within the middle digit.

Most of the animals studied showed prominent sagittal ridges in digits II and IV (Fig. 5B). This indicates that the outer digits offer more resistance to torsional loads, probably reflecting their main function as stabilizers during standing and walking, as well as their secondary weight-bearing function. Moreover, digit IV appears to have an even more accentuated sagittal ridge, which suggests that this digit, in particular, is usually under larger torsional moments than digit II. Thus the contribution of the digits to locomotion and support is unequal, and specifically is biased toward the midline of the pes in the animals studied.

The FEA study is consistent with observations of internal bone structure in these taxa. Compact bone lines the walls of convexo-concave phalanges (Fig. 8.1, 8.2), where the zones of highest stresses are found in the respective FEA models (Fig. 7.2B–D). Cancellous bone with small trabeculae is present close beneath the proximal joint surface (Fig. 8.1, 8.2), which is the same relative position as the elevated stresses (Fig. 7.2B–D). These small trabecular zones are underlain by a zone of larger trabeculae and a substantial medullary cavity (Fig. 7.2B–D), matching the location of a significant low-stress zone in the FEA model. In flattened phalanges, the trabecular architecture is more homogeneous, and compact bone is largely absent internally (Figs. 7.3, 7.4, 8.3, 8.4). These patterns closely match the loading distributions generated by our models.

Taken together, the alignment of the foot, trabecular structure, and loading distribution support the inference that the flattened phalanges of hadrosaurids reflect a marked modification of foot function from the primitive ornithopod (and dinosaur) condition. This transition involved a change

in pedal posture toward subunguligrady, restriction of flexion-extension movements, and homogenization of stress distributions and corresponding internal bony structures (see Fig. 10).

Function and Evolution of the Ornithopod Pes

Phalanges with highly convexo-concave joint surfaces are beneficial for bipedal animals. As they have only two supporting limbs, bipedal animals face greater structural requirements on the contact area of the pes, especially if it is to provide equilibrium for the entire body. It is possible to achieve this with long digits that exhibit high, controlled flexibility, thereby forming a "stabilizer platform." By contrast, quadrupedal animals are more stable (Muller and Verhagen, 2002) and therefore are capable of reducing the contact area of the foot. It is not a coincidence, perhaps, that no bipedal animal exhibits an unguligrade stance during free standing.

Flattened phalanges with narrow proximal joint surfaces, in combination with restricted mobility and upright posture, create a "columnar support," which represents the best structure for longitudinal (axial) loadings. This is also the best arrangement for bone resistance to compressive loading (Currey, 2002); thus this morphology would be able to support higher loads and be beneficial for larger-bodied animals. It seems logical, then, that large dinosaurs such as sauropods, ceratopsians, and stegosaurs, along with large mammals such as rhinocerotids and proboscideans, share this phalangeal morphology.

Another important feature for phalangeal function is the "neck" (see Fig. 5). This structure is a stress concentrator but also reduces the stress in other zones, especially the distal joint surface (compare between models in Fig. 7.1). In light of these results, small weight-bearing phalanges with a narrow neck seem improbable, because this small bone would have to support more loading per unit volume than a larger one, and the stress concentration in the phalanx neck could easily exceed bone resistance. Note that a small phalanx with a pronounced neck (Fig. 7.1C) exhibits the highest stress values of all the experiments. This might explain the reduction of the "neck" in derived pedal phalanges of ornithopods and other large-bodied animals.

The general shape of a bone is determined genetically. Nevertheless, as a living tissue, a bone responds to changes in loading by modifying its size, density, and internal arrangement (Currey, 2002). Thus, the final morphology of a bone depends significantly on its mechanical situation. This relationship between loading and bone structure was first recognized by Wolff (1870), and is popularly known as "Wolff's law of bone transformation." Although this so-called "law" has been challenged (Bertram and Swartz, 1991; Cowin, 1997), several studies have shown that in many cases trabecular structure tends to correlate with the direction of principal strains, while trabecular density and location of compact bone correlate with the magnitude of shear stresses (Hayes et al., 1982; Thomason, 1985; Lanyon, 1990; Biewener et al., 1996). Moreover, strains slightly higher than normal stimulate positive remodeling, and by contrast, lower routine strains lead to bone loss (Rubin and Lanyon, 1982). It is important to note that the internal structure of a bone does not present an optimal engineering design for loading, since this tissue has to deal with its vital cellular functions as well, such as gas, nutrient and waste exchange, as well as regulation of calcium availability. Therefore, bone structure reflects only general loading patterns. However, the identification of these patterns is important because it is usually

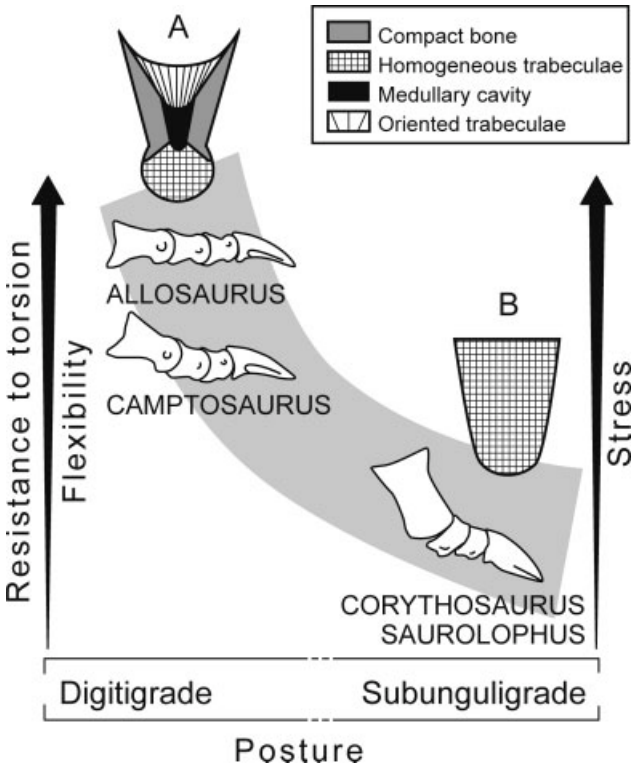

Fig. 10. Schematic summary of dinosaur phalanx morphofunction. **A**) sagittal section of a typically digitigrade phalanx (*Allosaurus* and *Camptosaurus*), which present a highly concave proximal joint, conically oriented trabeculae; "neck" with internal medullary cavity and external compact bone; and a highly convex distal joint with more homogeneous trabeculae. These features are associated to higher flexibility, resistance to torsion and stress. **B**) sagittal section of a typically subunguligrade phalanx (*Corythosaurus* and *Saurolophus*), which displays a more flattened (external) and homogeneous (internal) structure. These characteristics are related to lower flexibility, resistance to torsion and stress.

very difficult to determine what forces are acting on a bone or even less obvious what stresses are acting inside it.

When looking at the changes that occurred in ornithopod evolution, it is clear that on the line to Hadrosauridae, ornithopods drastically altered posture, changing the pes from a "stabilizer platform" to a "sub-columnar" structure. The associated soft tissues also altered their function. For digitigrade bipeds, pads act as energy-absorbing cushions and are typically digit-specific, but for subunguligrade quadrupeds, these digit pads became united beneath the pes and acquired an additional role in support.

CONCLUSIONS

This study examined the pedal phalanges of several dinosaurian taxa, as well as theoretical models of vertebrate phalanges. The results demonstrate correlative relationships between several aspects of external and internal pedal morphology, pedal posture, and bone loading. These suggest that the observed changes in pedal structure within ornithopod dinosaur evolution are indicative of significant alterations in foot posture and function.

Specifically, *Camptosaurus* and theropods (*Allosaurus*, *Rhea*, and *Dromaius*) exhibited many of the primitive (basal) conditions of the dinosaur foot: concavo-convex joints, marked processes for the attachment of the flexor and extensor tendons, excavated collateral fossae, a dorsal position of these fossae in the penultimate phalanges, a neutral extended claw, and weak sagittal ridges in the lateral digits.

In *Camptosaurus*, the presence of well-developed sagittal ridges in digit III (middle one) suggests that there was high flexibility in all digits, and possibly a mediolaterally asymmetric step. The weak development of the sagittal ridge in digit III of *Allosaurus* may indicate a more symmetrical step, but digit IV had higher flexibility, as evidenced from its strong joint curvature and marked sagittal ridge. Both ratites also show high joint curvature and development of the sagittal ridge in lateral digits, revealing a particularly elevated flexibility in digits II and III, and a symmetrical step, despite the stiffer digit IV. In general, digit III is the main weight bearer; lateral digits (II and IV) are under higher torsional moments, with digit IV being more strongly affected. Taken together, this suggests that locomotion in the specimens studied might have been biased toward the midline of the pes.

In contrast, hadrosaurids (*Corythosaurus* and *Saurolophus*) possessed a derived pedal morphology, including flattened phalanges, absence of collateral ligament fossae, and loss of processes for the attachment of flexor and extensor tendons. This morphology suggests that hadrosaurids had a more upright pedal posture than basal ornithopods, which was closely aligned to the main direction of the GRF during standing. Furthermore, the lack of a stress concentrator (phalanx neck) and the reduction of joint curvature allowed the hadrosaurid pes to support high loads more effectively than the primitive ornithopod pes.

FEA models show loading patterns that are consistent with trabecular structure, allowing us to assume that: primitive pedes (e.g., *Allosaurus* and *Camptosaurus*) are well-suited to work as "stabilizer platforms," which require high, controlled flexibility. On the contrary, derived pedes (i.e., hadrosaurids) are well adapted to "columnar support" and resistance to high loads.

Although this research was focused on certain dinosaurs, the functional morphological issues discussed here can be applied to other terrestrial tetrapods. Non-ungual phalanges are morphologically simple, but at the same time are directly relevant to numerous aspects of animal posture and behavior. This makes future comparisons between vertebrates especially promising with regard to problems of stabilization versus functionality, increasing body size, and postural changes during evolution.

ACKNOWLEDGMENTS

The authors thank Bruno Frölich and Evan Garofalo for their invaluable assistance in obtaining the CT scan data and Peter Kroehler for providing the ratite pedal bones used in this study. Emily Rayfield, John Hutchinson, Erick Snively, Colin McHenry, Biren Patel, Andrew Lee, Ryan Ridgely, Brian Richmond, Stephen Gatesy, Corwin Sullivan, Jennifer Scott, and two anonymous reviewers for providing constructive criticism in various aspects of the manuscript, and Stephen Wroe for further assistance.

LITERATURE CITED

Abourachid A, Renous S. 2000. Bipedal locomotion in ratites (Paleognatiform): Examples of cursorial birds. Ibis 142:538–549.

Alexander RM, Jayes AS, Maloiy GMO, Wathuta EM. 1979. Allometry of the limb bones of mammals from shrews (*Sorex*) to elephant (*Loxodonta*). J Zool 189:305–314.

Anderson JF, Hallmartin A, Russell DA. 1985. Long-bone circumference and weight in mammals, birds and dinosaurs. J Zool 207:53–61.

Bertram JEA, Swartz SM. 1991. The law of bone transformation—A case of crying Wolff. Biol Rev 66:245–273.

Biewener AA. 1989. Scaling body support in mammals: Limb posture and muscle mechanics. Science 245:45–48.

Biewener AA, Fazzalari NL, Konieczynski DD, Baudinette RV. 1996. Adaptive changes in trabecular architecture in relation to functional strain patterns and disuse. Bone 19:1–8.

Carrano MT. 1997. Morphological indicators of foot posture in mammals: A statistical and biomechanical analysis. Zool J Linn Soc 121:77–104.

Carrano MT. 1998. Locomotion in non-avian dinosaurs: Integrating data from hindlimb kinematics, in vivo strains, and bone morphology. Paleobiology 24:450–469.

Carrano MT. 1999. What, if anything, is a cursor? Categories versus continua for determining locomotor habit in mammals and dinosaurs. J Zool 247:29–42.

Carrano MT. 2001. Implications of limb bone scaling, curvature and eccentricity in mammals and non-avian dinosaurs. J Zool 254:41–55.

Carrano MT, Biewener AA. 1999. Experimental alteration of limb posture in the chicken (*Gallus gallus*) and its bearing on the use of birds as analogs for dinosaur locomotion. J Morphol 240:237–249.

Christiansen P. 2002. Locomotion in terrestrial mammals: The influence of body mass, limb length and bone proportions on speed. Zool J Linn Soc 136:685–714.

Cowin SC. 1997. The false premise of Wolff's law. Forma 12: 247–262.

Currey JD. 2002. Bones: Structure and Mechanics. Princeton: Princeton University Press. 436 p.

Dar FH, Aspden RM. 2003. A finite element model of an idealized diarthrodial joint to investigate the effects of variation in the mechanical properties of the tissues. Proc Inst Mech Eng Med [H] 217:341–348.

Dilkes DW. 2001. An ontogenetic perspective on locomotion in the Late Cretaceous dinosaur *Maiasaura peeblesorum* (*Ornithischia*: *Hadrosauridae*). Can J Earth Sci 38:1205–1227.

Farlow JO, Gatesy SM, Holtz TR, Hutchinson JR, Robinson JM. 2000. Theropod locomotion. Am Zool 40:640–663.

Gefen A, Seliktar R. 2004. Comparison of the trabecular architecture and the isostatic stress flow in the human calcaneus. Med Eng Phys 26:119–129.

Hayes WC, Snyder BM, Levine BM, Ramaswamy S. 1982. Stress-morphology relationships in trabecular bone of the patella. In: Galagher RH, editor. Finite Elements in Biomechanics. New York: Wiley. pp 223–267.

Heinrich RE, Ruff CB, Weishampel DB. 1993. Femoral ontogeny and locomotor biomechanics of *Dryosaurus lettowvorbecki* (*Dinosauria*, *Iguanodontia*). Zool J Linn Soc 108:179–196.

Henderson DM. 1999. Estimating the masses and centers of mass of extinct animals by 3-D mathematical slicing. Paleobiology 25:88–106.

Hildebrand M. 1988. Analysis of Vertebrate Structure. New York: Wiley.

Lanyon LE. 1990. The relationship between functional loading and bone architecture. In: DeRousseau CJ, editor. Primate Life History and Evolution. New York: Wiley. pp 269–284.

Levin SM. 2002. The tensegrity-truss as a model for spine mechanics: Biotensegrity. J Mech Med Biol 2:375–387.

Lockley MG, Hunt AP. 1995. Dinosaur Tracks and Other Fossil Footprints of the Western United States. New York: Columbia University Press. 338 p.

Matthewson MJ. 1982. The effect of a thin compliant protective coating on hertzian contact stresses. J Phys D: Appl Phys 15:237–249.

Middleton KM. 2003. Morphology, Evolution, and Function of the Avian Hallux. Providence, RI: Brown University. 167 p.

Muller M, Verhagen JHG. 2002. Optimisation of the mechanical performance of a two-duct semicircular duct system, Part 3: The positioning of the ducts in the head. J Theor Biol 216:443–459.

Paul GS. 1987. The science and art of restoring the life appearance of dinosaurs and their relatives. In: Czerkas SJ, Olson EC, editors. Dinosaurs Past and Present, Vol 2. Los Angeles: Natural History Museum. pp 5–49.

Reid REH. 1996. Bone histology of the Cleveland-Lloyd dinosaurs and of dinosaurs in general, Part I: Introduction to bone tissues. Bringham Young Univ Geol Stud 41:25–71.

Reilly DT, Burstein AH. 1975. Elastic and ultimate properties of compact bone tissue. J Biomech 8:393–396.

Rubin CT, Lanyon LE. 1982. Limb mechanics as a function of speed and gait: A study of functional strains in the radius and tibia of horse and dog. J Exp Biol 101:187–211.

Seebacher F. 2001. A new method to calculate allometric length-mass relationships of dinosaurs. J Vert Paleontol 21:51–60.

Sereno PC. 1999. The evolution of dinosaurs. Science 284:2137–2147.

Thomason JJ. 1985. The relationship of trabecular architecture to inferred loading patterns in the third metacarpals of the extinct equids Merychippus and Mesohippus. Paleobiology 11:323–335.

Wolff J. 1870. Über die innere Architektur der Knochen und ihre Bedeurung für die Frage von Knochenwachstum. Virchows Arch Pathol Anat 50:389–450.

Wright JL. 1999. Ichnological evidence for the use of the forelimb in iguanodontid locomotion. In: Unwin DM, editor. Cretaceous Fossil Vertebrates Special Papers in Paleontology, Vol 60. Oxford: Blackwell publishing. pp 209–219.